Design and Simulation of an Active Thermal Cooling System for Lithium-ion Battery Pack for Portable Pulsed Power Loads

Bryan Kelly
Applications Engineer, Staff
Synopsys, Inc
Hillsboro, OR 97124
Email: bryan.kelly@synopsys.com

Abstract **— Energy Storage Systems (ESSs) can be applied to compact portable pulse power systems such as electromagnetic railguns (EMRGs), and high-power laser directed energy weapons (LDEWs). In mobile land, shipboard, or submarine applications, available energy and thermal management are key design concerns. Lithium-ion batteries compared to traditional lead-acid, have the highest current values of specific energy and are more efficient, consequently are well-suited to implementation in high-power or high-energy configurations. With the ever-increasing size and design complexity of the Li-ion battery pack for energy demanding applications, the protection, performance, integrity, and longevity of the battery is of increasing concern to Government and Defense organizations as electrification becomes more widely deployed in the field. Battery life can suffer from premature aging or degradation due to the heat generation, particularly during fast charging and discharging cycles. The internal heating and capacity of Li-ion batteries is strongly dependent on the discharge rate, with higher discharge rates increasing internal heating and reducing the available capacity. Moreover, semiconductor laser diode arrays (LDA) used in LDEWs, may draw 100kW or more and generate a lot of heat. Excessive heating and thermal cycling play a key role to limit the reliability and lifetime of LDAs.**

In this paper, a high-level simulation study will be presented to illustrate virtual prototyping of an active cooling system for maintaining the temperature of an Li-ion battery pack and pulse power driven LDA load. Active cooling was designed as a complementary system, utilizes a coolant circulated via a motor driven thermohydraulic pump, through pipes, a crossflow heat exchanger and cooling plates resident against the battery pack and the LDA assembly. A programmable thermostat coupled to a needle valve maintains the temperature of the dynamic thermal Li-ion battery pack within a narrow but optional Goldilocks region of operation. In face of range of ambient temperatures, and heavy load scenarios, an active liquid cooled system gives the most effective and efficient thermal management to ensure safety and optimal battery life, validated through stress and statistical simulation analyses.

Keywords— Energy storage, lithium, li-ion battery pack, batteries, railgun, laser, ESS, EMRG, LDA, LDEW, thermal hydraulics, pulsed power, stress analysis.

I. INTRODUCTION

The development of compact pulsed-powered devices is of continuing interest and the high power and energy density in Lithium-ion (Li-ion) energy storage devices present an opportunity to use these technologies in portable implementations. High-power semiconductor laser diode arrays (LDAs), are widely used in military defense and industrial applications, [1], [2]. However, a drawback is LDAs are very expensive and heat-vulnerable, and the quality of the emitted laser is greatly affected by the pulse power supply [3] [4] and available battery energy. The overall integrity of the pulsed power supply and Li-ion battery pack operating at the required current demands is at the mercy of significant heat generation. Long-term operation implies the Li-ion battery pack will adamantly require charging at appropriate times, and rapid charging control also generates heat that requires appropriate alleviation. Failure to do this will shorten both battery and LDA life and will eventually compromise nominal operational behavior. The focus of this paper is to design and assemble a complete compact pulsed-power LDA system with liquid cooling for the purposes of high-level evaluation. Once a working system is constructed, it can serve as the executable spec to tighten down more specific design requirements. The battery back will be sized, and an AC/DC charger and charge control algorithm will be implemented and tested.

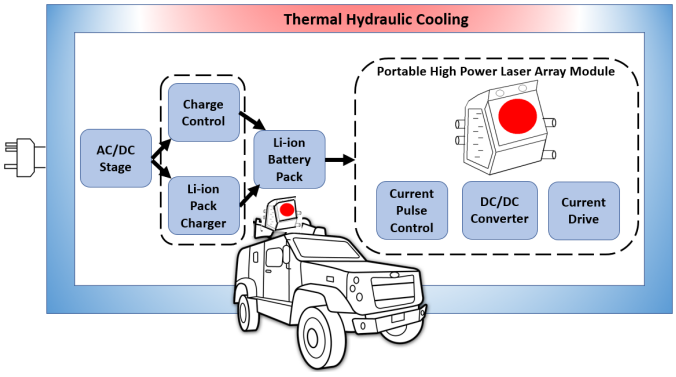

Fig. 1: Concept of complete of a portable pulsed-power LDA system.

A block diagram of the system is shown in figure 1. The Li-ion battery pack is the prime power source and embedded within the thermohydraulic cooling loop. The battery pack charger and

LDA module also generate heat and require cooling. The charge controller monitors the pack temperature, charging current, AC input voltage, power consumption, etc. and will shut down if any integrity or safety thresholds are crossed. The AC/DC stage is the input stage of the charger, and more details of all these sub-assemblies are described in the body of this paper. Figure 2 illustrates the virtual prototype for entire system assembly.

In this paper, SaberRD, a multi-domain simulation tool will be used. A self-heating Li-ion battery model will be characterized from typical manufacturer available performance data, and a battery pack will be sized against an estimated LDA load. A high-level LDA model will be assembled and also sized according to the application requirements. The LDA module with DC/DC converter, current pulse generation and drive will be shown, accompanied with its thermohydraulic cooling plate. Since the portable application generally implies a mobile installation platform, the vehicle's already present standard Ethylene-Glycol cooling system availability can be utilized, but not required, as the portable pulsed-power LDS system liquid cooling can also be self-contained. Since battery energy is not infinite, an OBCM (On-Board Charging Module) will be presented as a 2-stage AC/DC and DC/DC converter. The overall thermohydraulic modeling and temperature regulation will be reviewed. Finally, simulation results for different aspects of the system will be shown.

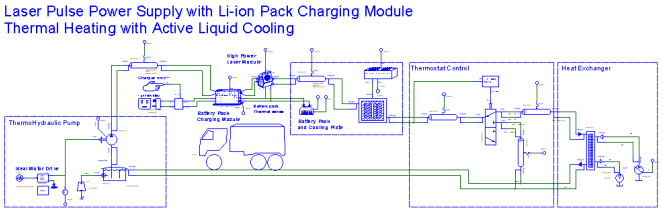

Fig. 2: Virtual prototype of a complete portable pulsed-power LDA system.

This paper is organized as follows. In section II, models for LDA and Li-ion devices under study are assembled based on available datasheet information. A brief overview of a 2-stage on-board-charger module (OBCM) is introduced in section III. In section IV, the modelling of the overall pulsed-power LDA system assembly and thermohydraulic active cooling control is presented. In section V, simulation results and observations are presented. Conclusions are given in section VI.

II. LDA AND BATTERY MODEL

The laser is operated in quasi-continuous wave (QCW) mode, which functions at relatively low duty cycle, typically 100-300 µs pulse length, 1 Hz to 1 kHz pulse frequency, where the pulse current is clean without overshoot [6]. The laser diode selected is produced by Northrop-Grumman corporation. A single BAR and V-I characteristic curve are shown in figure 3.

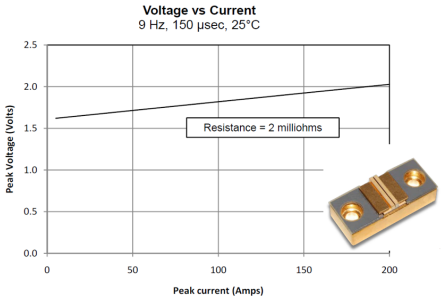

Fig. 3: ARR179P200 curve. Courtesy of Northrup-Grumman

As shown, the laser diode does not fire unless the applied voltage is $\geqslant$ 1.6V, and the resistance of a single BAR is 2 mΩ. Therefore, if a pulse current of 150A is applied, the amplitude of the pulse voltage is, 150A * 2 mΩ + 1.6V = 1.9V. The pre-determined design requirement was 310 BARs in series, so this places a ballpark nominal battery pack voltage at ~590V for the DC-link rail. We will frame-up the battery pack model next.

LiFePO4 battery chemistry was selected as a protection measure for this system as can safely sustain high current discharge rates. The disadvantage is it has a low nominal 3.2V and 3.65V maximum charge, so more cells will be needed, compared to say, LiCoO2 chemistry, which has a 4.2V maximum voltage but much less tolerant to charge/discharge stress [5]. The LFP26650P appeared to be a good fit, shown in figure 4, and the next step is to determine the row-column configuration of the battery pack.

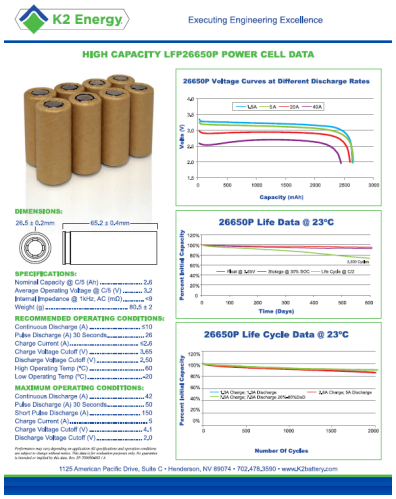

Fig. 4: . LFP26650P LiFePO4 battery cell datasheet. Courtesy of K2 Energy.

The estimated 192 number of LFP26650P cells in series allows a nominal 614 Volt pack, and was determined from three key factors; the laser diode BAR pulse current drive amplitude, the number of BARS in series in the LDA assembly, and the nominal 3.2V cell voltage and lowest battery pack SOC that will permit reliable operation. The process to characterize a single cell and generate a battery pack is a trivial one thanks to the SaberRD battery tool. See figure 5.

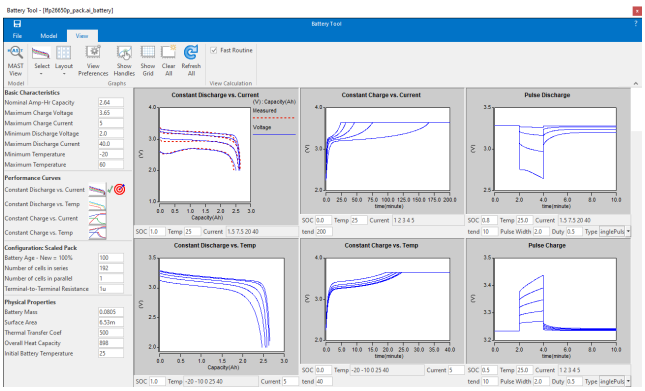

Fig. 5: . SaberRD battery tool characterized to LFP26650P with battery pack size specified.

The manufacturer given discharge curves are entered, and the battery tool automatically fits via an internal optimizer. Moreover, in absence of other performance data, which is a common occurrence and may be an expensive process to obtain, such as discharge and charge data w.r.t. temperature, the tool will estimate all other characteristics. Consequently, the battery simulation model from the get-go is physically realistic, and what you see here in the tool is what you get. This takes the mystery out of how the battery model will perform in the virtual prototype of the system design. Admittedly there is a concern that the 2.5 Ah cell capacity may not be sufficient to permit adequate field operation before recharging the Li-ion battery pack would be required. The addition of columns of cells in the pack assembly would resolve this concern, albeit does come at a price of more cells, hence elevates size, cost and weight. Back of napkin calculations can be performed to estimate the theoretical overall pack capacity required based upon the current pulse amplitude and frequency, etc. But Li-ion cells can be expected to arrive for pack assembly with intrinsic calendar aging, and to ensure maximum lifespan are typically operated within 80% to 20% SOC region. However once the cell model is characterized, it is a trivial matter to plug-n-play the pack model electrical row-column configuration in the SaberRD battery tool, which includes self-heating and aging effects.

Prior we discussed the LDA to permit sizing of an appropriate battery model, but now return to the LDA to assemble a simulation model for this device. This is straightforward as the laser BAR essentially operates as a diode, and a PWL diode model turn-on and intrinsic capacitance parameters can be scaled by the number of BARs in series. The self-heating behavior was derived by the diode's small series resistance which transmutes the electrical power into thermal power. A 1st-order passive thermal network represents the thermal mass of the BAR assembly, of which is bolted upon an adjacent liquid cooling plate as shown in figure 6. The LDA requires clean and precise current pulses. A DC/DC converter provides galvanic isolation from the battery pack and an appropriately sized output stage capacitance, which holds adequate charge to dump energy into the LDA. Accurate voltage-to-current control is permitted by current measurement feedback. Figure 6 illustrates the complete LDA module model.

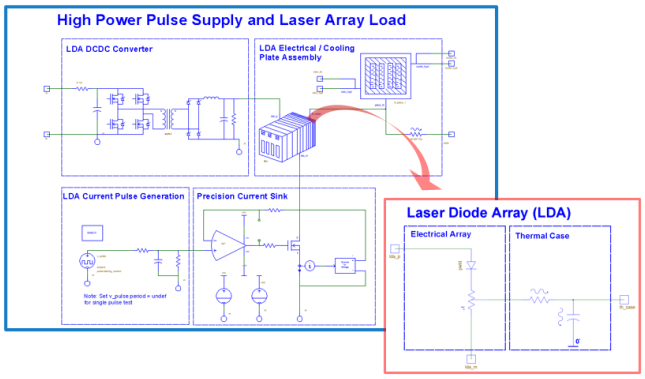

Fig. 6: . LDA Module; LDA, DC/DC converter, pulse current drive, and thermal cooling

III. Pulse Supply Li-ion OBCM Model

OBCMs generally include two power converters. Input power from the ac-grid, is passed into to an ac/dc converter. This converter transforms ac voltage to pulsating dc voltage and boosts the voltage to an intermediate value (typically 400 V). The second converter is an isolated dc/dc converter, and a large capacitor between the two converters is required to filter the ac grid frequency. The DC/DC converter transforms the intermediate voltage to the final output voltage required for battery charging. Figure 8 illustrates the complete charger system implementation of the OBCM; however, we can refer to figure 7 to observe a simplified block diagram.

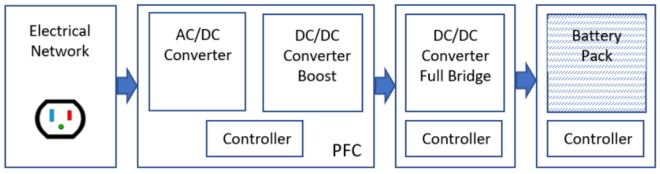

Fig. 7: Simplified Block Diagram of OBCM.

Anything plugged-into the electrical grid must minimize reflection of harmonics back onto the grid, and this is the objective of PFC, Power Factor Correction. The front-end (AC/DC) converter rectifies AC grid voltage and boosts it to an intermediate voltage (approximately 400 V). International standards require the OBCM to maintain a high-power factor and limit harmonic currents at the ac mains. Multiple topologies are suitable for the required power range. As illustrated in figure 8, a PFC is a converter that consists of an AC/DC input rectification stage, followed by a DC/DC converter, boost in this case. An important feature of PFC control is a voltage sensor which measures the output load voltage, and a current sensor which measures the inductor current in the boost converter. As an interleaved boost concept was adopted here, two inductor currents are sensed for feedback purposes. Using this information, PFC control can be realized. An averaged model of an interleaved PFC boost front-end stage offers flexibility to determine general functional behavior, before tightening down onto more detailed hardware specifications. Many conventional circuit averaging techniques provide a simple method for the

formulation of averaged, equivalent circuit models such as Vorperian's PWM Switch Model [7].

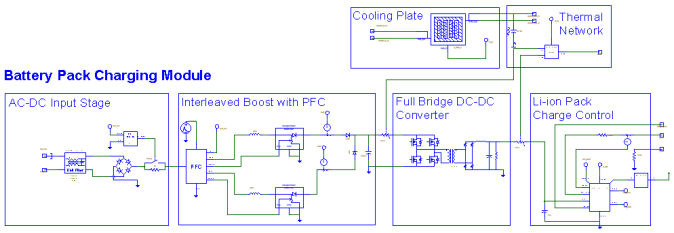

Fig. 8: Virtual Prototype of Pulse Supply OBCM.

The full-bridge DC/DC converter consists of a switching H-Bridge or half-bridge, whose output feeds into a coupling transformer, usually 1:1 ratio to provide galvanic isolation and convert the switching DC to AC interpretation. This is then passed through a diode full bridge to translate a DC output from the converter. The DC level ultimately realized from the converter is obtained via a voltage control loop feedback that commands via a fixed or variable switching frequency with duty-cycle commands exercises the front-end switching devices. To reduce simulation overhead, an average model of a Full-Bridge DC-DC converter was derived from [8, 9] and its state space model is shown in (1)-(6). In this circuit and model there are two state variables; inductor current and capacitor voltage, and examination of two different modes of operation and KVL and KCL allows the averaged converter to be derived as:

$$\dot{X} = AX + BV_{in} \quad [1]$$

$$V_{out} = CX \quad [2]$$

$$A = \begin{bmatrix} -\frac{2R_{th}d + r_D(1-2d)}{L} & -\frac{1}{L} \\ \frac{1}{C} & -\frac{1}{RC} \end{bmatrix} \quad [3]$$

$$B = \begin{bmatrix} \frac{2dn}{L} \\ 0 \end{bmatrix} \quad [4]$$

$$C = [0 \quad 1] \quad [5]$$

Where…

$$R_{th} = 2n^2 r_{sw} + 2r_D \quad [6]$$

The charge controller implements an electrically isolated precision current sink that leverages measurement of the battery current as feedback in a simplistic voltage-2-current control circuit. Usage of a self-heating MOSFET as a variable resistance introduces implicit voltage-to-current mode transition when the source sensed current, translated as a voltage signal, rises to the commanded battery charger current level. The charging current will consequently roll-off when the battery approaches charged state. The charge control algorithm makes decisions based on presence of ac power, battery pack temperature, specification of power the OBCM can deliver, and actively monitors both battery pack voltage and current to set the charge operational state, and eventually shutdown, when commanded charge level reached. A 12 Volt energized, high voltage contactor (HVC) and control circuit is enabled only if a power-on digital signal (VAC good) is true. A manual ON/OFF switch, shown in figure 2, provides indication that the mobile platform has returned to base and been plugged into the ac-grid to recharge the battery pack.

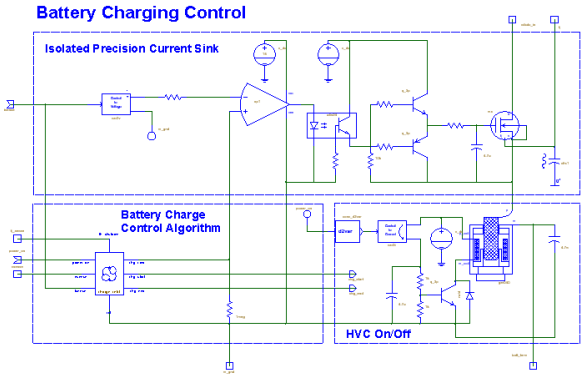

Fig. 9: Charge controller assembly.

The algorithm shown in figure 11, was implemented in the SaberRD StateAMS tool; see figure 10. StateAMS allows the creation of mixed-signal finite state machine models from a language independent description based on state charts and equations. State charts are a powerful visual formalism for capturing complex system behavior at a high level of abstraction in the early stages of a design. StateAMS has the unique ability to relate state-based behavior closely to conserved systems.

StateAMS produces models in MAST and VHDL-AMS. Being intuitive and requiring little training, the tool removes much of the burden associated with the subtleties of the modeling languages. Structured code and the ability by non-modeling experts to easily review the models are some of the benefits found in using StateAMS. The tool facilitates the creation of behavioral models for power management control algorithms or electrical control units.

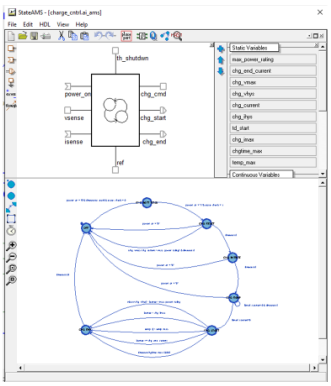

Figure 10 : Charge Control Algorithm of OBCM implemented in StateAMS.

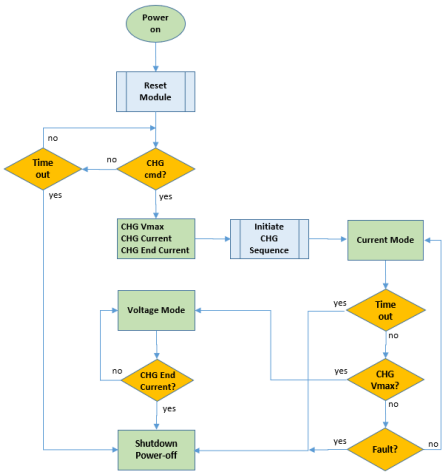

Figure 11 : Charge Control Algorithm of OBCM Battery Charger.

IV. THERMOHYDRAULICS MODELING

A battery generates heat when it is charged and discharged, and thermal management ensures that a battery operates within a narrow Goldilocks region of operation (e.g. 30 – 35 °C). This safeguards performance, longer life, and a healthy reliable battery pack. Therefore, thermal management is essential to consider, and this may take the form of either passive or active cooling, the latter is generally a combination of both. An active cooling system is less sensitive to the external environment and therefore offers flexibility for a portable pulsed-power system. A general overview is shown in figure 12. As a side note, since charging of a frigid Li-ion cells is detrimental to battery life performance, it is important to first elevate the battery temperature sufficiently. Most Li-ion cells cannot be fast-charged when they are less than 5 °C and should not be charged at all when they are below 0 °C. Battery pack heating options will be discussed as future work.

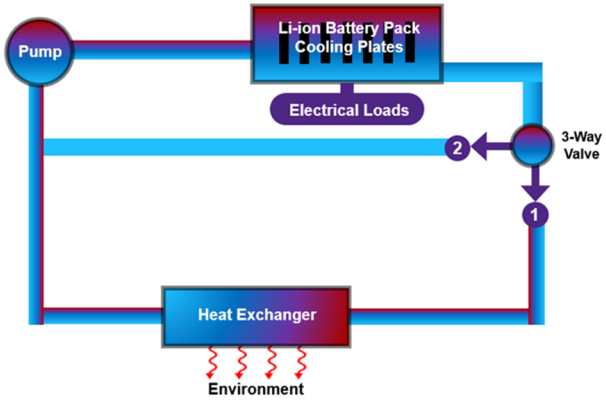

Figure 12: Active cooling overview.

On the far left is the cooling pump to provide the displacement and pressure to move the coolant to-and-fro. This delivered coolant is passed around the Li-ion battery pack via an adjacent cooling plate, figure 13. The heat generating electrical loads, LDA and the OBCM also participate in the liquid cooling. A thermostat auto-adjusts the coolant flow between a bypass line and through the heat exchanger. The thermostat is coupled to a 2-position, 3-way, mechanically operated valve controlled by the thermostat's control. All these thermal hydraulic design elements are be modeled w.r.t. to energy conservation principals and were characterized according to geometry aspects of each device. Models of thermal hydraulic elements are based on the following fundamental laws.

Mass flow rates must balance (flow continuity)

$$\frac{dm_{cv}}{dt} = \sum_n g_n = 0 \qquad [7]$$

Energy rate must balance (First Law of Thermodynamics):

$$\frac{dU_{cv}}{dt} = Q_{cv} + h_i g_i - h_e g_e - W_{cv} \qquad [8]$$

System continuity principles "always" apply:

$$\sum_n \Delta p_n = 0 \quad \sum_n \Delta T_n = 0 \qquad [9]$$

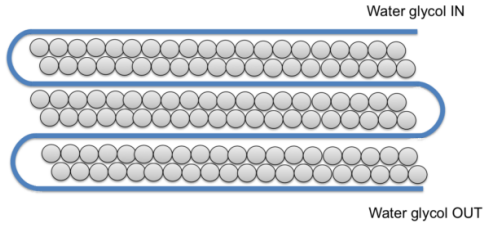

Figure 13: Example cooling plate illustration.

The complete assembled system is shown in figure 14. An ideal pump motor and drive is used to rotate the hydraulic pump. This alleviates substantial simulation overhead without changing the behavior of the pump thermal hydraulics. The pump itself is a model that aligns with standard datasheet parameters. At the heat exchanger, heat flow convection via a fan or forced airflow, where air temperature at the entrance or front of the mobile vehicle is also considered. Heat flow generated from the battery pack, LDA, and OBCM is absorbed via a distributed cooling plate, and are subjected to a passive thermal network, figure 18, to provide heat flow to ambient via conduction and emissivity. The coolant temperature on the output of the cooling plate is sensed, brought to the thermostat, which internally compares that to a programmable specified reference temperature, the error signal generated combined with amplifier output drives the mechanical linkage connected to the 3-way spool valve. The translational range of motion of the valve's mechanical shaft is +/- 0.005 meters.

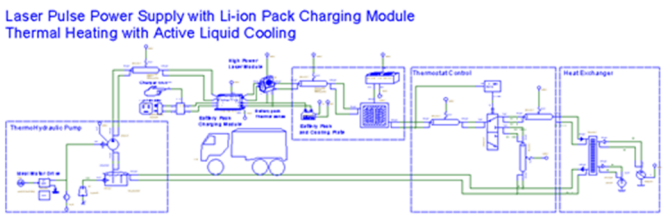

Fig. 14: Virtual prototype of a complete thermal hydraulics active cooling system for LDA pulsed-power supply

We have the “system” but it needs “coolant” as this is the mechanism that provides heat flow via its intrinsic mass and fluid characteristics. The age-old vital importance and role of coolants & refrigerants in heating, ventilation, and air conditioning systems, has driven large community efforts to encapsulate a thorough understanding of the behavior properties of many industry standard coolants and refrigerants. Important fluid thermodynamic and transport properties, and where applicable, their mixtures have been captured in large table databases [10,11]. Figure 15 shows the imported Ethylene-Glycol behavior using the SaberRD TLU tool in SaberRD. And the tables embrace density, enthalpy, specific heat capacity, viscosity, and thermal conductivity vs. temperature and mixture ratio. With data availability that describe the coolant in entirety over temperature “and” mixture ratio, the characterization effort is minimized, and one has the additional insurance that coolant behavior properties inserted into the thermal hydraulic models are captured very precisely.

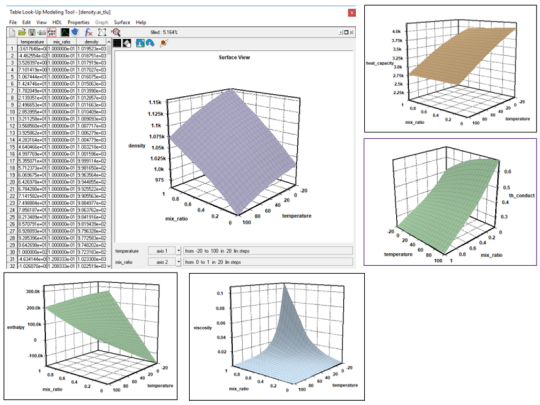

Figure 15: Coolant Modeling and Characterization.

Basically, all physical systems and, especially, pneumatic, magnetic, hydraulic, and thermal systems are distributed parameter systems, and partial differential equations are the typical form in their description. However, design and simulation of physical systems in “PDEs” requires enormous resources across the board, consequently modeling, characterization. and simulation overhead is a burden. And that overhead potentially decouples one from the system-level perspective. A lumped system however implies the dependent variables of interest are a function of time alone. In general, this will mean solving a set of ordinary differential equations (ODEs), and algebraic expressions. In other words, the PDEs have been discretized or reduced to ODE equivalence. Space does not permit detailed descriptions of all elements, so for brevity purposes a pipe element is shown in figure 16.

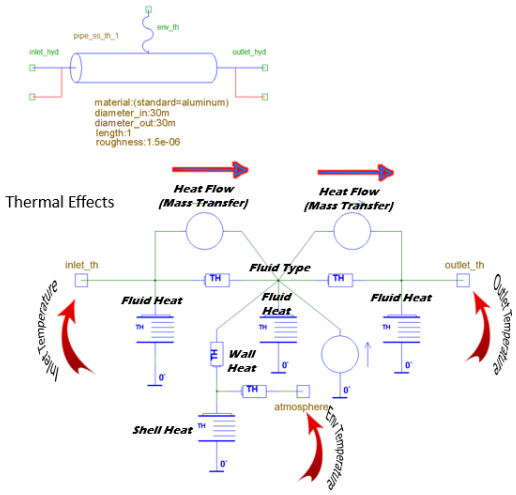

Figure 16: Fluid Dynamics Modeling; pipe example.

The model of a component (pipe or other) must have as many hydraulic ports as there are hydraulic connections. Fluid volume is distributed depending on the model. Observe orifices may be used to model various effects, for example difference in inlet and outlet pipe diameters. And with the pressure, and hydraulic losses in place, we will have physical realistic hydraulic flow. Every hydraulic port is accompanied by a thermal port through which heat energy is conveyed due to mass transfer and fluid enthalpy. There are as many thermal ports as there are heat exchange paths with the surroundings. The pipe model embraces hydraulic flow, pressure drop, thermodynamic effects, heat transfer due to coolant-pipe convection, etc., but there are other fluid mechanics features need to consider in the model. For example, boundary w.r.t. laminar and turbulent flow shown in figure 17.

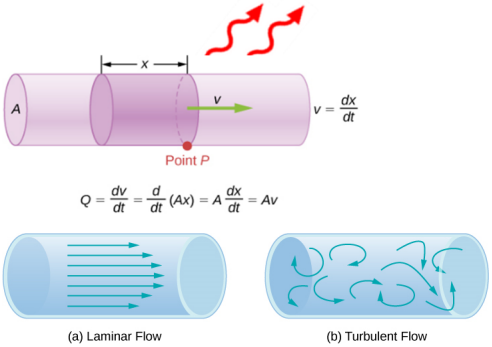

Figure 17: Consideration of boundary conditions.

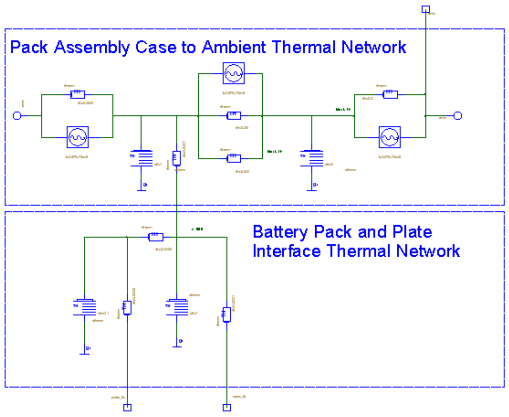

Figure 18: Example model of passive cooling via conduction and emissivity to ambient.

V. Results

Once a design concept is captured in entirety as a virtual prototype, it allows validation of nominal behavior, but also lends enormous flexibility to plug-and-play with design attributes to investigate the design to make certain it will meet the application of intent. Thereby, the virtual prototype serves as an executional spec. The shaped current pulse applied to the LDA was decided to be 150A, 200us, with 10us rise and fall times, however the applied burst frequency expected to be variable ranging from 10 to 30 Hz.

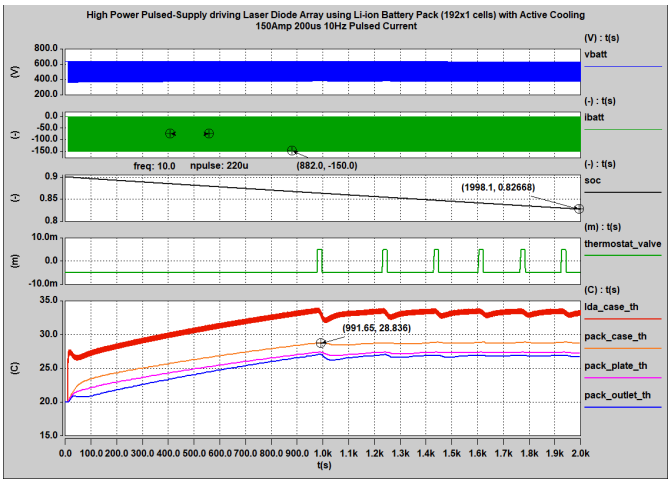

Figure 19: Active-cooled pulsed-power supply under thermal regulation with 150Amp LDA load

Figure 19 shows the pulsed-power supply under thermal regulation. This illustrates nominal operation with 10 Hz current pulsed applied to the LDA. The system goes into thermal regulation against the heat produced by both the LDA and Li-ion battery pack. The coolant temperature on the output of the cooling plate is sensed, brought to the thermostat, which internally compares that to a programmable specified reference temperature. The internal error signal generated combined with amplifier output drives the mechanical linkage connected to the valve. The thermostat activates the 3-way valve to divert coolant from the bypass to-and-through the heat exchanger. The coolant releases heat to ambient environment via fan cooling. Because of several degrees of offset between the slightly higher averaged battery pack case temperature and the cooling plate output temperature, the thermostat temperature offset is set to 27 °C.

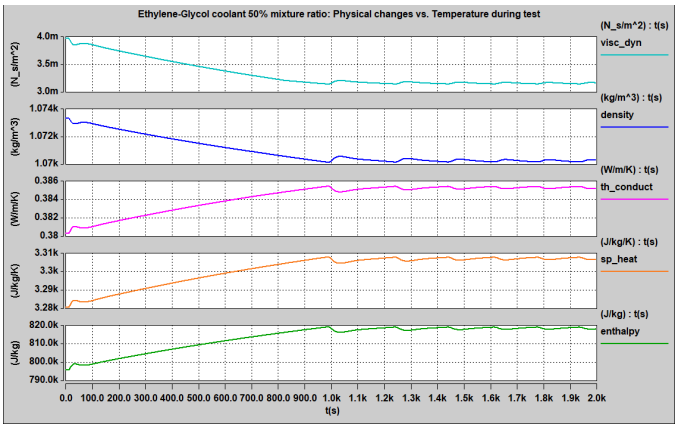

Figure 20: Ethylene-Glycol coolant (50% mixture ratio) operating characteristics vs. temperature under nominal test

The coolant properties change under temperature as shown in figure 20. Illustrated are dynamic viscosity (kinematic viscosity not shown), density, thermal conductivity, specific heat (Cp), and enthalpy. The behavior is modulated thanks to active control. A pertinent validation aspect of the system simulation is the pressure drop across the coolant plate. For this unit an expected pressure differential was around 1-2 kPa. Figure 21 shows a reasonable ballpark for a first pass and one can go back and fine tune the cooling plate characterization to bring about a better fit.

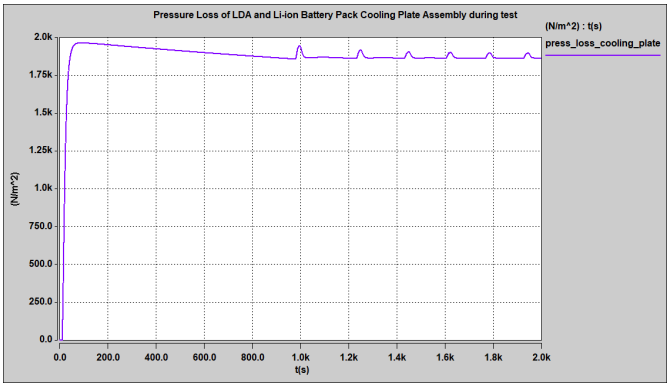

Figure 21: Pressure drop within LDA and Li-ion battery pack coolant plate

A virtual prototype is very useful to validate nominal behavior, but invaluable as an active executional spec to investigate variances that could potentially adversely impact the system design behavior. SaberRD has a full suite of design analysis tools at the user's fingertips to employ as needed, ranging from Fault Analysis, Multi-Vary Analysis, Worst-Case Analysis (WCA), Experiment Analyzer, and much more. All these tools can be applied to any design under study to ensure the system is robust. Once the high-level design is working appropriately, top-down design techniques can be leveraged to introduce details to respective portions to bring about greater physical fidelity. The rule-of-thumb is Galls' Law which states,

"A complex system that works is invariably found to have evolved from a simple system that worked. The inverse proposition also appears to be true: A complex system designed from scratch never works and cannot be made to work. You have to start over, beginning with a working simple system."

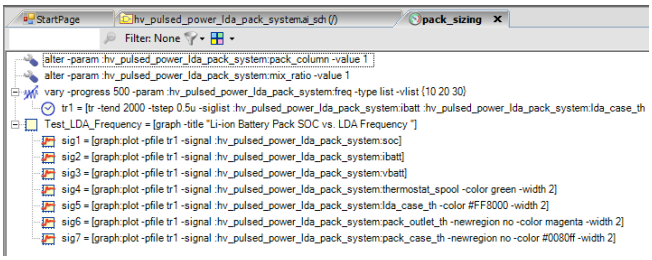

Figure 22: Experiment set-up in SaberRD

Figure 22 shows the battery pack sizing test set up in the Experiment Analyzer. While a functional vary of number of columns could have also been introduced this was temporarily removed to help visualization of the following results in figure 23. Here the LDA burst frequency again was applied as an interval of 16 minutes, but swept at the values 10 Hz, 20 Hz, and 30 Hz. Temperature rise in the LDA and battery pack was observed, but thermal regulation kept the averaged battery pack temperature under 35 °C. According to Northrup-Grumman datasheet, the laser diode bar has a maximum operating temperature of 70 C, so this still resides within SOA (Safe Operating Area).

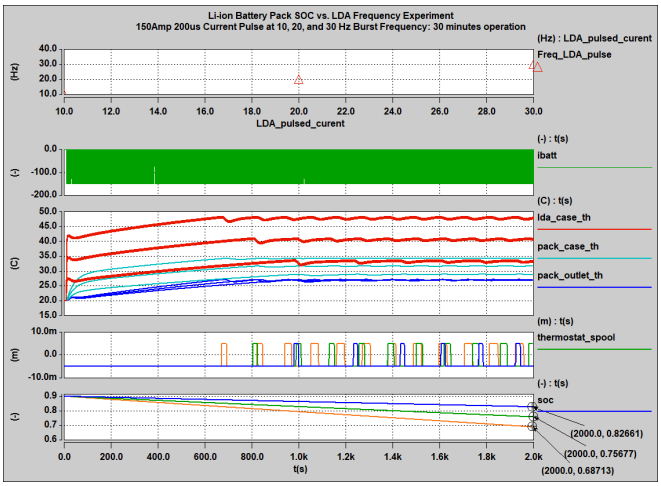

Figure 23: Active-cooled pulsed-power supply tested at 150Amp LDA pulsed-current frequency sweep.

What is of concern however is the battery pack SOC dropped nearly 25% for 16 minutes of 30 Hz operation. If the unit is to be employed as a portable unit in the field, for days or weeks, which may not have immediate access to AC-grid to permit charging, this may be detrimental to application intent. Even if an AC/DC converter is available upon the vehicle transport platform, to cease operation to permit recharge of the Li-ion pack may not be practical. The addition of another column of cells in parallel with the 192 cells in series will linearly extend the pack capacity and the operational time accordingly. For example, if the pack size was increased to 192x2 cells, and the test rerun, one will observe the SOC drop will be in the order of 12.5%. As another experiment verification step, the Ethylene-Glycol and water coolant mixture ratio was investigated and system tested at 40%, 50% (nominal), and 60%. See figure 24.

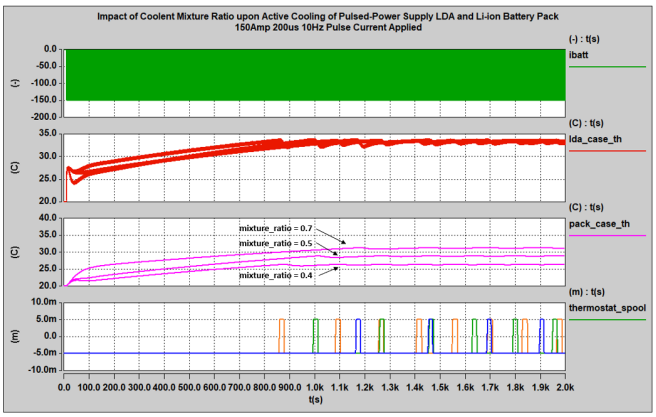

Figure 24: Ethylene-Glycol mixture ratio tested at 40%, 50%, and 60%

Raising the Ethylene-Glycol percentage in the coolant will raise the fluid's viscosity and density, which in turn decrease its heat transfer and heat carrying properties. Cp drops as the mixture ratio goes up, so one expects things to run hotter at 60% mixture for the same fluid temp and flow rate, meaning the coolant would be able to carry away less heat at 60% as opposed to 40% mixture ratio. The price paid for avoiding freezing is in the Cp. But if the cooling plate is running hotter, then as observed in figure 24, the battery pack case temperature is also running hotter. This could pose a concern if fan windage observed at the radiator is low or the vehicle motion is not adequate or in the face high ambient temperatures, which could be high as 40 °C. Investigative adjustments to the cooling plate fluid volume, inlet and outlet diameters will allow more assurance w.r.t. SOA.

It is important to validate the pulsed-power supply OBCM against the Li-ion battery pack. Figure 25 illustrates an applied nominal charge current command of 8.0 Amps. While demonstrates an entire charge cycle, for brevity the battery pack was set to an initial SOC of 80%. The battery pack accepted current begins to roll off as it slowly charges up. The charge controller algorithm will shut down when the battery current reaches the specified minimum charge roll-off current of 4 Amps, or under several fault conditions. For example, if the battery temperature exceeds a maximum temperature of 45 °C. To verify the controller algorithm over-temperature management works properly, the hydraulic pump was turned-off. Thereby the only cooling available is passive in nature w.r.t. the thermal conductive and emissivity network to ambient; see figure 18. Although the charging current was applied as a constant current for simplicity as opposed to a pulse-train, passive cooling appears it may not be sufficient against a 5600 W charger (3.65 Vmax/cell * 8 A * 192 cells). This will require investigation to ensure robustness and safety.

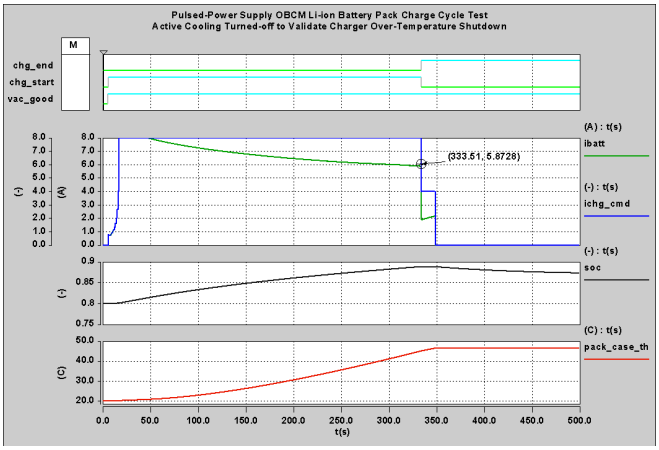

Figure 25: Li-ion battery pack OBCM test: Over-temperature shutdown.

The pulsed-power supply OBCM design was modified slightly to permit start-up in 0.1 seconds to permit easier closer scrutiny of the PFC behavior. It was then simulated for 2 seconds to acquire data to determine if meets design performance expectations. The charge current was set to a maximum of 8.3 Amps as a worse case check. Refer to figures 26 and 27 for an examination of performance.

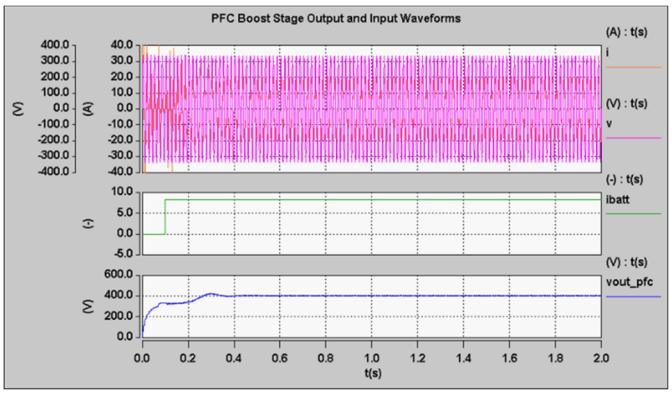

Figure 26: Simulation of PFC and input and output signals.

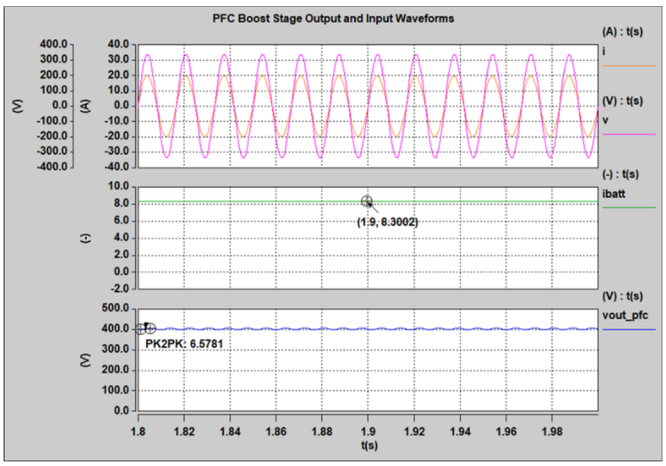

Figure 27: Zoomed to show current and voltage relationship.

The modeling of the PFC stage was briefly discussed prior, and a detailed dive into the particulars would require another paper in-itself. However, under maximum charging load, the PFC shows alignment of the voltage and current signals, and these measurements can next be leveraged to calculate the output power, efficiency, and THD of the OBCM.

VI. Conclusions

In conclusion, a complete Li-ion battery pack powered HV pulsed power LDA system was assembled and tested. Albeit the system is of high-level abstraction, it is intended as a working platform to permit the introduction of increasing levels of design details. For example, the system requires a smarter thermostat, which employs a variable set-point based on different sensed operating conditions (e.g. mixture ratio, ambient temperature, fan or vehicle speed) and so on. Clearly further granularity of the battery pack and cooling plate will permit additional fidelity of thermal measurement feedback and control. Assuming the pack design resides with 192x1 cells, 12 modules of 16 cells each could be broken out and altogether placed against a distributed cooling plate assembly as shown in figure 28. If the cost versus benefit of a larger battery pack is warranted, then the module size could be increased to 32 cells. The scaling of the battery module size is simple process once the cell is characterized in the SaberRD battery tool. The 3-way spool valve can also be updated to a rotary ball valve. There are different options in the SaberRD thermal hydraulic library.

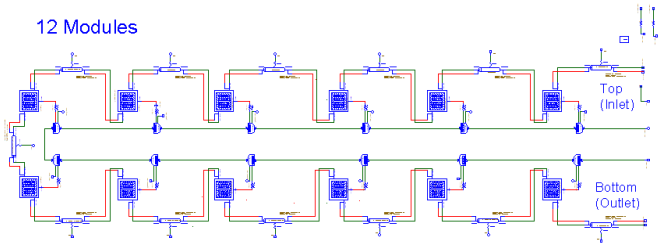

Figure 28: Concept of battery pack modules adjacent to distributed cooling plate.

Even if the hardware prototype was available it may not be practical nor possible, to test and measure all the possible variations of performance over a large multidimensional parameter space. But if simulation via a virtual hardware prototype accurately captured the implementation concept, worst-case scenarios and corner cases could be efficiently investigated in face of any random or user selected combination of device and system variations. The benefits of virtual prototyping can be immediately tangible, particularly when the systems are more complex with different types of interacting technologies. The simulation model of the design can serve as an indispensable executable specification early in the design phase and final design verification. Moreover, statistical analysis would provide insight to both validate and elevate the system robustness in face of component tolerances due to manufacturing process variations.

About Synopsys

Founded in 1986 in North Carolina, USA, Synopsys is now among the “Top 15” largest software companies in the world and a world leader in the areas of Electronic Design Automation (EDA), Technology Computer Aided Design (TCAD), and Software Quality, Integrity and Security (APPSEC) tools and services. Headquartered in Mountain View, California, Synopsys employs over 14,000 engineering and support staff around the world.

References

[1] [1] J. Qiu, K. Liu, and Y. Wu, ``A pulsed power supply based on power semiconductor switches and transmission line transformer," IEEE Trans. Dielectr. Electr. Insul., vol. 14, no. 4, pp. 927_930, Aug. 2007.

[2] J. Wojtanowski, and M. Zygmunt, M. Traczyk, Z. Mierczyk, and M. Jakubaszek, ``Beam forming optic aberrations' impact on maximum range of semiconductor laser based

[3] E. Penovi, R. G. Retegui, S. Maestri, G. Uicich, and M. Benedetti, ``Multistructure power converter with h-bridge series regulator suitable for high-current high-precision-pulsed current source," IEEE Trans. Power Electron., vol. 30, no. 12, pp. 6534 6542, Dec. 2015.

[4] S. C. Kim, H. Heo, C. Moon, S. H. Nam, D. S. Kim, S. S. Park, J. H. Kim, S. S. Oh, J. W. Yang, and J. H. Sho, ``Optimal design of 40-kV longpulse power supply," IEEE Trans. Plasma Sci., vol. 44, no. 4, pp. 694 701, Apr. 2016

[5] Battery University, “BU-205 Types of Lithium ion”, 22 Oct. 2021, https://batteryuniversity.com/article/bu-205-types-of-lithium-ion

[6] M. Kanskar, J. G. Bai, Z. Chen, W. Dong, S. Elim, X. Guan, M. DeVito, M. Grimshaw, and S. Zhang, ``High ef ciency kW-class QCW 88x nm diode laser bars," in Proc. Conf. Lasers Electro-Opt., 2012, pp. 36

[7] V. Vorperian, "Simplified analysis of PWM converters using model of PWM switch. Continuous conduction mode," in IEEE Transactions on Aerospace and Electronic Systems, vol. 26, no. 3, pp. 490-496, May 1990.

[8] Ghadimi, Ali & Rastegar, Hassan & Keyhani, Ali. (2019). Development of Average Model for Control of a Full Bridge PWM DC-DC Converter.

[9] C. Iannello, Shiguo Luo and I. Batarseh, "Small-signal and transient analysis of a full-bridge, zero-current-switched PWM converter using an average model," in *IEEE Transactions on Power Electronics*, vol. 18, no. 3, pp. 793-801, May 2003.

[10] Bell, Ian H. and Wronski, Jorrit and Quoilin, Sylvain and Lemort, Vincent, Pure and Pseudo-pure Fluid Thermophysical Property Evaluation and the Open-Source Thermophysical Property Library CoolProp, Industrial & Engineering Chemistry Research

[11] Lemmon, E.W., Bell, I.H., Huber, M.L., McLinden, M.O. pages.nist.gov › REFPROP-docs